Antimisting Fuel Kinematics Related to Aircraft Crash Landings

Anthony San Miguel*
Naval Weapons Center, China Lake, Calif.

An approximate analysis is presented to quantitize kinematic behavior of antimisting Jet A fuel in an airstream representative of survivable aircraft crash landings. Antimisting fuel data were generated from a fuel expulsive airfoil placed in an airstream adjacent to a pulsing propane flame. Measurements of burning front velocities and accelerations were obtained from a camera located within the airfoil. These data were used in the analysis to predict the diameter, shear stress, and shearing strain rate of the average particle of antimisting fuel in the airstream under the airfoil. A description is given of the airflow-airfoil apparatus in the context of its simulation of crash landing conditions. The feasibility of using antimisting agents to suppress a fuel fire during a crash landing is evaluated.

Nomenclature

a_{ave} = average acceleration of flame front, cm/s^2
a_b = flame front acceleration, cm/s^2
a_p = acceleration of average fuel particle, cm/s^2
A_1 = area, cm^2
C = coefficient of drag
C_F = skin friction coefficient
d = diameter of average fuel particle, cm
D = drag, dyn
f = cumulative frequency of occurrence, %
g = acceleration due to gravity, 9.8 m/s
h = vertical distance between airfoil and fuel hopper, m
l = length of cylindrical fuel particle, cm
N_R = Reynolds number based on cross-sectional area
Re = Reynolds number based on particle surface area
t_i = time of crash impact, s
v = relative velocity of average fuel particle to airstream, cm/s
v_a = relative velocity of airstream to flame front, cm/s
$(v)_{ave}$ = average flame front velocity, cm/s
v_b = flame front velocity, cm/s
v_c = airflow velocity under airfoil camera, cm/s
V = initial landing velicity, knot
ΔV = wing velocity change due to impact, knot
V_h = fuel flow velocity due to intrinsic fuel head, m/s
V_w = relative velocity of wing to ground, knot
x = wetted surface length, cm
$\dot{\gamma}$ = shear strain rate, s^{-1}
$\dot{\epsilon}$ = normal deformation rate, s^{-1}
η_S = shear viscosity, dyn-s/cm^2
η_T = tensile viscosity, dyn-s/cm^2
θ = angle between flight direction and particle radius vector, deg
μ = viscosity of air, dyn-s/cm^2
ρ_a = density of air, g/cm^3
ρ_l = density of antimisting fuel, g/cm^3
ρ_w = density of air adjacent to fuel particle, g/cm^3
τ = maximum shear stress on fuel particle, dyn/cm^2

Introduction

A RECENT review[1] of the antimisting fuel literature shows that antimisting agents are effective for fire suppression of low volatility fuels (JP-5, JP-8, Jet A) under many testing conditions of high air-shear exposure. An existing problem is to relate laboratory experiments utilizing rheological and chemical kinetic models,[2] so as to predict the results from qualitative "in the field" tests[3] using proprietary agents of unknown origin. An approximate analysis is presented in the paper to address this problem.

The precise physical mechanism(s) by which polymeric antimisting agents exert their influence on fuel fire suppression is still subject to conjecture. Although it is believed that antimisting effectiveness is primarily influenced by shear force action, other factors may also influence its effectiveness. For example, chemically induced fire inhibitions related to heat transfer mechanisms are not yet well understood for dynamic environments characterized by transient phenomena. One could argue that the problem cannot be defined and solved in the foreseeable future. On the other hand, by introducing a number of subjective assumptions, it is possible to synthesize an approximate analysis to reasonably quantify the complex phenomena. The particular air-shear loading environment considered in this paper is unique to a particular in the field test[3] that is representative of antimisting behavior under an aircraft wing sustaining a passenger-survivable crash landing.

The dynamics of passenger-survivable aircraft crash landings are not well known.[4] Data from such crashes for fixed-wing transport aircraft are limited to deceleration potentials in the cockpit/cabin. Much of aircraft crash dynamics must therefore be hypothesized on the basis of judgment, applying approximations to the principles of mechanics. With this input, an airflow-airfoil test apparatus was scaled to generate antimisting effectiveness data. Then, by utilizing various engineering approximations, it was possible to generate kinematic and shear loads intrinsic to antimisting fuel particle behavior in turbulent airflows, representative of those under a wing experiencing a survivable crash landing.

Aircraft Wing Crash Dynamics

It is presumed that a pilot attempting a survivable crash landing will choose as level a landing site as available and attempt to minimize his landing velocity. If unavoidable obstacles are in the landing path, the pilot probably will attempt to impact them so as to prevent cartwheels, overturning, or direct cockpit collision. The crash scenario envisioned results in aircraft crashes shown in Ref. 3. With these assumptions, the crash dynamics of an aircraft wing can be approximated by assuming that deceleration data obtained

Received Feb. 28, 1977; revision received Dec. 27, 1977.

Index categories: Fuels and Fuel Systems; Multiphase Flows; Safety.

*Mechanical Engineer. Member AIAA.

for masses within a fuselage can be directly applied to masses (fuel) in the wing. Data given in Ref. 4 can then conservatively be used to predict the change in wing velocity, ΔV, occurring during the impact time t_i, associated with any given impact in terms of percentage cumulative frequency of occurrence, f, for $30\% < f < 90\%$, by

$$\Delta V = 0.592[0.44f + 20] \quad (1)$$

$$t_i = 0.031[0.44f + 20][0.079f + 3.1]^{-1} \quad (2)$$

These equations were obtained by curve fitting Figs. 1-19 and 1-22 of Ref. 4, and inserting those relationships into Eq. (9) of Ref. 4. To illustrate Eqs. (1) and (2), if $f = 90\%$, $\Delta V = 35.3$ knot, and $t_i = 0.181$ s.

Of interest in this study is the relative velocity of the wing to the ground, V_w, after initial impact of the wing (leading to fuel spillage). Initial landing velocities at San Francisco Airport can be approximately by curve fitting percentage cumulative frequency of occurrence data[5] to obtain

$$V = 0.39[f + 315.4] \quad (3)$$

For $f = 90\%$, 158 knots can be used for typical commercial transport. It follows by subtraction of Eq. (1) from Eq. (3) that $115 < V_w < 123$ knot for crash landings between $30\% < f < 90\%$.

The fuel within the wing ejects out of a hole in the leading edge (due to impact/collision)[3] with a velocity ΔV greater than V_w. This ejected fuel is subjected to drag and gravity. Depending on the aerodynamic drag vs wing drag (due to the crash), it is possible that the fuel will only eject forward of the wing.[3] The time frame to expect the fuel to flow at ΔV greater than V_w is of the order of t_i, after which $\Delta V \rightarrow V_h$, where V_h is the fuel flow velocity due to the intrinsic fuel head in the wing. As the aircraft comes to rest $V_h \rightarrow V_w$, assuming, of course, that there is still fuel in the wing. Obviously as $V_h \rightarrow V_w$, a greater percentage of the spilled fuel will travel below and behind the leading edge of the wing. It will further be assumed that ignition sources are predominantly found behind and below the leading edge of the wing. If the average intrinsic fuel head is taken as 3 m, then $V_h = 7.8$ m/s.

In this study, the aircraft wing crash dynamics were restricted to those aft and under the leading edge for $99 < V_w < 143$ knots and $V_h = 7.8$ m/s.

Airflow Facility and Airfoil Apparatus

Air temperature significantly affects the ignition and sustenance of fuel fire because of heat transfer mechanisms, ignition susceptibility of the fuel, and vapor generation mechanisms related to inflammable fuel/air ratios. Since antimisting agents presumably do not increase the flash point temperature of the neat fuel, the highest airflow test temperature need not exceed the minimum flash point temperature (40.5°C).

A low-velocity diffuser was designed and built to provide an airstream with a square cross section of 90.5 cm on each side. The design was optimized for 100-knot flow, although its dynamic range is between 0 and 200 knots. Figure 1 illustrates the diffuser design. Temperature-controlled (±0.2°C) supersonic air is brought from an existing blowdown storage facility into the aft end of the diffuser by means of a 15.3-cm-i.d. steel pipe 9.5 m long. The length of the diffuser is 6.1 m. The aft square cone housing is 1.83 m long, 1.6×1.6 m square aft, and 0.86 m forward (each side converging 12 deg). Contained in the center of the square cone is the diffuser element. It consists of a 1.83-m-long cylinder whose periphery consists of a 12-pointed star with an o.d. of 45.7 cm and an i.d. of 38.1 cm. The thickness of the steel cylinder wall is 0.95 cm. There are 72 2.54-cm-diam holes symmetrically located on the periphery. A 30.48-cm-long cone caps one end of the diffuser element. A 1.22-m-long mixing

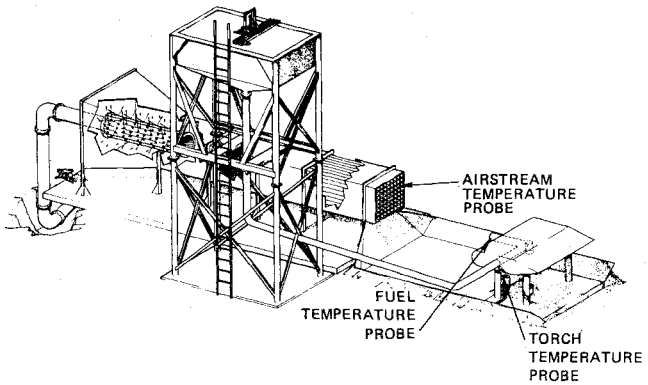

Fig. 1 Low-velocity diffuser-airfoil test facility.

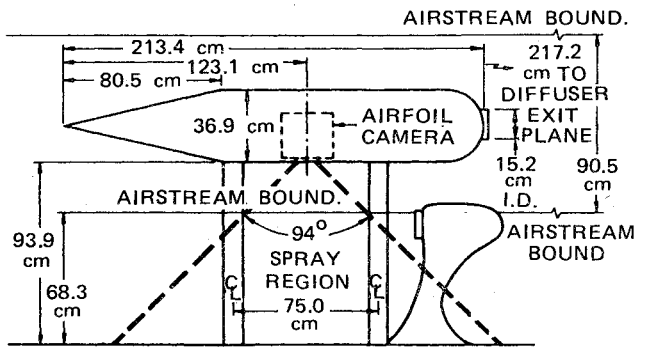

Fig. 2 Airfoil configuration in relationship to airstream and propane igniter.

section was bolted to the square cylinder. This was, in turn, attached to a 0.61-m-long square section containing six screens of 2.54 and 1.77 cm wire mesh. These screens are placed in pairs 30.48 cm apart. Next, another 91.4-cm-long mixing section was bolted on. Finally, a 1.52-m-long section, containing egg crate configuration straighteners (each cell is 109 cm^2) was bolted to the adjacent mixing section.

Pilot probe surveys of the airflow documented that the longitudinal velocity turbulence was less than 10% and homogeneous to within 5 knots, with a repeatable velocity within 5% from test to test for airstream velocities between 100 and 150 knots.

The dimensions of the airfoil from which antimisting fuel was ejected into the airstream are shown in Fig. 2. This airfoil was placed 217.2 cm aft of the diffuser exit plane (see Fig. 1). The airfoil chord, thickness, and length were 213.4, 36.9, and 152.4 cm, respectively. In the leading edge, midway along the length, protruded a 15.2-cm-i.d. tube. This tube was attached to the fuel hopper 325 cm above the airfoil. The airfoil was 93.9 cm above the ground and was placed in the center of the diffuser. Leakage rates could be controlled to some degree by the release plunger in the fuel hopper. In this study, leakage rates (dump rate density) were between 0.14 and 0.34 1/s-cm^2.

A propane torch was located along the lower airflow boundary. This ejected on command a finite propane flame (approximately 1000 cm^3 volume) along the lower airstream boundary (see Fig. 2).

Within the airfoil was located a 16-mm camera housed in a water jacket. A wide-angle lens (3 mm) was used that was protected by a quartz window. The actual viewing field was 94 deg (shown in Fig. 3) with pertinent dimensions to correct for distortion (see also Fig. 2).

Airflow velocity attenuation data are given in Fig. 4 under the airfoil for airstream velocities between 100 and 150 knots. Note the significant attenuation and increase in turbulence aft of the leading edge. The velocity data behind the leading edge were obtained during the pilot probe survey with the airfoil

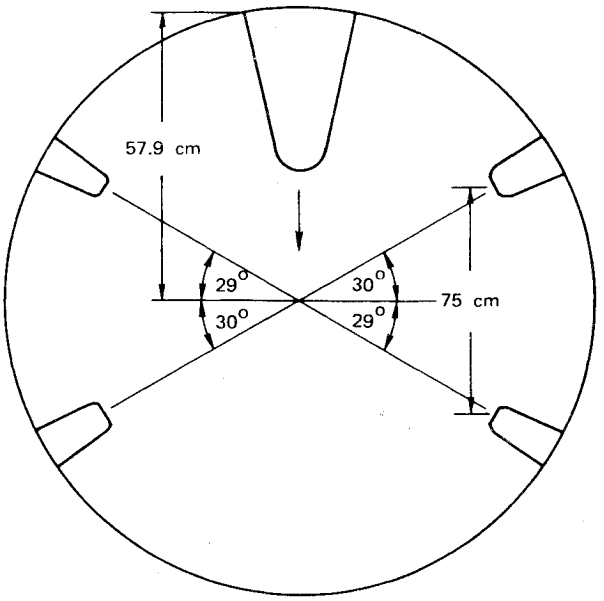

Fig. 3 View recorded by airfoil camera.

placed in the airflow, as shown in Fig. 2. The data are valid at 81 cm above the ground reference, but do not incorporate any obstructed flow effects that would be introduced by fuel interaction phenomena. Since the maximum fuel dump rate used in this study resulted in maximum fuel-to-air volume ratios of the order of 10^{-3}, it is assumed that obstructive flow effects are not significant in comparison with the airflow instabilities that are introduced by the airfoil placed within the airstream.

Antimisting agents were carefully mixed with Jet A fuel to avoid any possible shearing degradation. Fuel blending was performed in a 208-l drum placed on a 340-kg-capacity scale. The antimisting concentrate was added to the neat fuel by gravity flow until the appropriate weight concentration was achieved. The resulting liquid components were then mixed at ambient temperatures (about 24°C) with a wooden paddle until the anticipated viscosity was reached. This generally required less than 10 minutes of mixing. The antimisting fuel was then stored for less than a week prior to the test. The temperature-conditioned antimisting fuel was then gravity-fed to the fuel hopper (Fig. 1). Temperature conditioning of the fuel was done by temperature-controlled electric blankets.

Antimisting Fuel Tests

Two significantly different antimisting agents were tested: AM-1 produced by CONOCO, Inc., and FM-9 produced by Imperial Chemical Industries, Ltd. Each of these agents was mixed in 0.3% by weight proportions in Jet A fuel. FM-9 was also mixed in 0.4% by weight proportions in Jet A fuel. The physical characteristics of 0.3% AM-1 differ from 0.3% FM-9 in that the former prevents misting by breaking up into long, stringy, spiderweb-like geometries when entrained by the airflow (see Fig. 10, Ref. 2); whereas the latter breaks up into unattached long, stringy elements, together with both elongated and short ellipsoidal liquid particles (see Fig. 9, Ref. 2).

Both antimisting agents were shown to be effective fire-retardant agents in numerous tests using the apparatus previously described. Tests are currently in progress to establish a failure envelope in the context of optimization. Figure 5 illustrates a failure envelope for FM-9 concentrations between 0.3 and 0.5% using diffuser exit plane airflow velocities between 100 and 170 knots. These data were obtained for fuel and airflow temperatures of 27 and 32°C, respectively. Conditions above the failure envelope signify complete fire extinguishment. Conditions below the failure envelope signify various degrees of fire retardation, including tests in which both pass and marginal fire pulses were observed. To eventually obtain a complete failure envelope will require the development of an analytical model to relate results from a finite number of tests. The first step to reach this long-range goal is to synthesize an approximate analytical model. The analytical model developed later requires data for the velocity and acceleration of a fire flame front in the airstream from tests which were judged to extinguish the applied fire. Therefore, the only test data presented in this paper are for tests in which the airfoil camera recorded a fireball that either self-extinguished or passed through the field of view (Fig. 3) and remained in the airstream.

Data for ten fireballs from successful tests are given in Table 1. The diameters of these fireballs ranged between 2-10 cm. Tests 1-3 are for 0.3% AM-1, tests 4-8 for 0.3% FM-9, and tests 9 and 10 for 0.4% FM-9. The first six columns identify the test conditions. The next column, v_c, is the airflow velocity under the airfoil camera and was obtained from Fig. 4. The average flame front velocity, $(v)_{ave}$, was obtained from the airfoil 16-mm film, based on a film reference distance of 64 cm (the edge of the airflow, Fig. 2). The flame front velocity fluctuated smoothly, but was always positive. The average was obtained by adding the velocity computed from each frame and dividing by the number of frames. The next column, v_a, is the difference between the airstream velocity and the average flame front velocity. By utilizing common graphical techniques, curves were generated through the velocity data resulting in well-behaved computed accelerations, the average of which are given in the last column. The judged accuracy of the data in the table is inferred by the significant figures used.

Particle Kinematics

Kinematic models of particles generated by air entrainment in liquid sheets must, of necessity, be approximations of a most complex process. Particles traveling in airstreams in the vicinity of an airfoil are subjected to recirculation eddies with

Table 1 Fireball kinematic data for 0.3% AM-1 and 0.3, 0.4% FM-9

Test no.	Agent	Airstream temp., °C	Fuel temp., °C	Dump rate density, 1/s-cm^2	Airstream velocity, knot	v_c, m/s	$(v)_{ave}$, m/s	v_a, m/s	$(a)_{ave}$, m/s^2
f 1	AM-1[a]	27.2	26.7	0.31	126	55.09	11.87	43.22	8.6 1
2	AM-1[a]	22.2	30.6	0.32	101	47.50	10.26	37.24	2.6
3	AM-1[a]	22.2	30.6	0.32	101	47.50	10.85	36.65	149
4	FM-9[a]	26.8	28.2	0.14	99	46.19	3.87	42.32	60
5	FM-9[a]	26.8	28.2	0.14	99	46.19	5.04	41.15	81
6	FM-9[a]	27.2	33.3	0.21	140	56.23	43.35	10.88	114
7	FM-9[a]	27.8	29.4	0.32	122	53.54	7.87	45.67	−67
8	FM-9[a]	27.2	26.7	0.32	122	53.54	14.61	38.93	−485
9	FM-9[b]	28.3	28.9	0.30	122	53.54	14.82	38.72	138
10	FM-9[b]	26.7	26.7	0.34	143	57.43	21.42	36.01	−328

[a]0.3% [b]0.4%

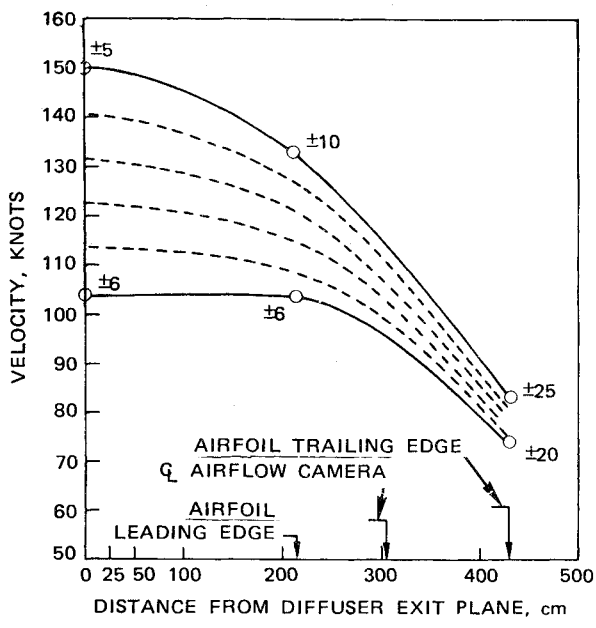

Fig. 4 Airflow velocity attenuation.

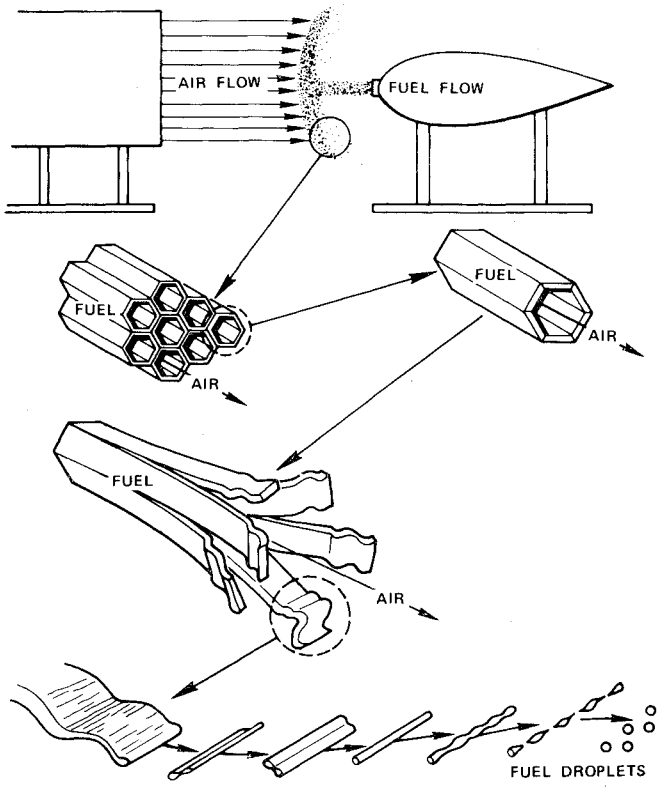

Fig. 5 Failure envelope for FM-9 antimisting fuel for fuel and airflow temperatures of 27 and 32°C, respectively.

both forward and reverse flow, which are associated with regions of high shear and high intensity of turbulence. Therefore, the engineering model to be developed, in order to be tractable, deals with approximations of averages of significant measurable variables.

A careful study of movie and still film of the flow patterns emanating from the airfoil test apparatus suggests the overall flow model shown in Fig. 6. In essence, a fuel stream ejects out of the leading edge of the airfoil with a velocity of $\sqrt{2gh}$, where h is the vertical distance between the airfoil and fuel reservoir. Interaction with the airstream results in a three-dimensional umbrella air entrainment geometry. The en-

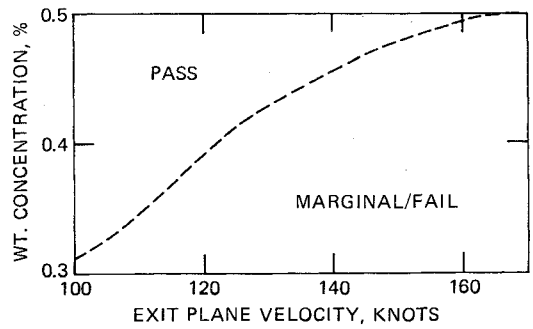

Fig. 6 Model of antimisting fuel kinematics.

trained air is decelerated and fuel accelerated along streamlines. Eventually, the air breaks through the liquid as represented by the honeycomb structure, which has no particular theoretical basis, but is utilized as a convenience. The walls of this conceptual structure are assumed to be liquid fuel. The walls of the hypothesized honeycomb structure separate at the seams and interact with neighbor elements that are capable of forming three-dimensional spiderweb-like networks. The web elements then reduce to droplets using a droplet formation model, such as proposed by Dombrowski[6] for a liquid sheet. That portion of the geometric model applicable to the region under the airfoil depends on the concentration of the antimisting agent. In this study, 0.3% AM-1 and 0.3%, 0.4% FM-9 fuels are approximated by infinitely long cylinders. No attempt is made to predict the conditions for sheet instabilities leading to cylinder generation.

The drag D on a liquid cylindrical particle in an airstream is approximated by

$$D=0.25\pi d^2 l\rho_l a_p \tag{4}$$

where the liquid particle is defined as a right circular cylinder of length l, diameter d, and density ρ_l. The acceleration a_p is that of the particle.

The coefficient of drag is defined by

$$C=D(0.5A_l\rho_a v_a^2)^{-1} \tag{5}$$

where A_l is the cross-sectional area of the cylinder, ρ_a is the air density, and v_a is the velocity of the airflow with respect to the particles. Since $A_l = ld$, substitution of Eq. (4) into Eq. (5) yields

$$C=\pi\rho_l a_p d/2\rho_a (v_a)^2_{\text{ave}} \tag{6}$$

It will be assumed that the average longitudinal velocity of a flame front witnessed by the airfoil camera is that of the average particle. The assumption is based on the observation that large particles downstream of the fireball travel at velocities close to that of the observed fireball flame front. This observation is particularly evident when the fireball extinguishes itself within the camera field of view, e.g., tests 1 and 4-6. Utilization of this assumption is reasonable if the velocity of the particle, v_p, is great with respect to the burning velocity, v_b, i.e., $v_p \gg v_b$. A large range of apparent burning velocities are reported in the literature that apply to neat fuels exhibiting phenomena based on molecular, thermal expansion, and other effects. For example, when neat Jet A is used in the test apparatus, the preceding effects create a serious explosion. Such apparent burning velocities never occur when antimisting agents are used (0.15% is the lowest concentration used by the author). Furthermore, much evidence was found with antimisting fuels that larger ignited particles move downstream with no apparent propensity to exhibit phenomena observed for neat fuel. Therefore, burning velocity data in the literature, addressing unusual neat fuel burning phenomena, are believed not to be pertinent to

burning phenomena of antimisting fuels. The largest v_b reported[7] for the various hydrocarbon/air flames that would be expected to exist in a jet fuel fire is about 50 cm/s. Thus, for velocity data obtained with an accuracy of 10%, the condition $v_p \gg v_b$ is met if $v_p > 500$ cm/s. From the data in Table 1, the condition is met; hence, it will be assumed that $v_p = (v)_{ave}$. In the same vein, the average particle acceleration $(a_p)_{ave}$ can be approximated as equal to the flame front acceleration a_b. With these assumptions, Eq. (6) can be used to obtain a relationship between C and d that must be satisfied.

If the relative velocity between that of the average particle and the surrounding air is known, then a second relationship that must be satisfied is

$$N_R = v d \rho_a \mu^{-1} \tag{7}$$

Again, using the assumption that $v_p = (v)_{ave}$, it follows that

$$v = v_c - (v)_{ave} = v_a \tag{8}$$

Substituting Eq. (8) into Eq. (7) and using Table 1, the relationship between N_R and d is determined.

The relationship between C and N_R is unique[8] for a cylinder; hence, d may be obtained by trial-and-error using Eqs. (6) and (7). The computed values for d are given in Table 2 for each test. Intrinsic assumptions made during the measurement time domain are numerous. They include assumptions that flow is normal to the particles, that the particles do not evaporte, that interactions among the particles do not occur, and that an average particle can characterize a distribution.

The range for 0.3% AM-1 is $150 < d < 5500$ μm, for 0.3% FM-9 it is $34 < d < 273$ μm, and for 0.4% FM-9 it is $80 < d < 120$ μm. These relative magnitudes are consistent with magnified photographs of larger particles observed for 0.3% AM-1 and FM-9. Care should be taken in interpreting the significance of d. It should not be used directly as a measure of fire-suspression effectiveness. Its value for a given antimisting agent is that the larger it is the fewer the number of small particles in the airstream. It is apparent that average particle size in itself is not the only factor contributing to fire suppression. For example, a given concentration of AM-1 is much more effective in reducing apparent fuel misting qualities than FM-9. But FM-9 is much more effective to suppress fire on the basis of utilizing much smaller particle sizes to attain the same level of effectiveness as the larger particle sizes intrinsic to AM-1. Perhaps the reason relates to particle distributions below 10 μm, i.e., FM-9 has a smaller population than AM-1. Note that the average particle size of neat Jet A is less than 1 μm. In any event, it is reported elsewhere[9] that in certain kerosine/air burning experiments, 95% of the liquid volume in a spray was in droplet sizes below 80 μm. Hence, the predicted values for d appear reasonable as an estimate of the average antimisting particle diameter.

Table 2 Predictions of average diameter, shear stress, and strain rate of cylindrical antimisting fuel particles

Test no.	d, μm	Re, $\times 10^6$	C_F, $\times 10^{-3}$	τ, dyn/cm^2	$\dot{\gamma}$, s^{-1}
1	1907	40.22	2.2	23.4	468
2	5500	99.95	1.9	15.2	304
3	150	2.68	3.2	24.8	496
4	303	6.26	2.8	29.0	2900
5	203	4.08	3.0	29.7	2970
6	38	0.20	4.6	31.7	3170
7	273	6.08	2.8	33.8	3380
8	34	0.65	3.9	34.5	3450
9	120	2.27	3.2	27.6	2760
10	80	1.41	3.5	26.2	2620

With d known, it is possible to estimate the average shear stress on the average particle by utilizing the power law for the skin friction coefficient, C_F, using the Falkner constants[10]

$$C_F = 0.0262 Re^{-0.1429} \tag{9}$$

The Reynolds number is defined here as

$$Re = \rho_w v_a x / \mu \tag{10}$$

where ρ_w is the air density adjacent to the fluid particle and x is the wetted surface length on the particle. It was shown[10] that x can be estimated by

$$x = 0.5 d \tan\theta \tag{11}$$

where θ is the angle between the flight direction and the radius vector. Furthermore, it was shown that the maximum shear stress τ along the periphery of a sphere occurs at $\theta \sim 56$ deg. Substituting this value into Eq. (11) and combining Eq. (11) with Eq. (10) yields

$$Re = 0.7413 (\rho_w v_a d / \mu) \tag{12}$$

Re is computed using v_a (Table 1) and d (Table 2) and is listed in Table 2. Given Re, C_F is computed from Eq. (9) and listed in Table 2.

The shear stress is given by[10]

$$\tau = 0.5 C_F \rho_a v_a^2 \tag{13}$$

Substitution of C_F from Table 2 and v_a from Table 1 into Eq. (13) yields τ, which is listed in Table 2. The intrinsic assumptions used to estimate τ include, in addition to those made to compute d, that heat transfer mechanisms can be neglected and that the computed maximum shear stress will occur over the entire surface because of the particle being a liquid.

The shear viscosities, η_s, of 0.3% AM-1 and 0.3% FM-9 in Jet A at 20°C are about 0.05 and 0.01 poise, respectively. By assuming Newtonian behavior within a specified domain of non-Newtonian behavior, the shear strain rate $\dot{\gamma}$ is given by

$$\dot{\gamma} = \tau \eta_s^{-1} \tag{14}$$

Substituting τ from Table 2 and the appropriate η_s yields $\dot{\gamma}$ from Eq. (14), which is listed in Table 2. The predicted values show that $\dot{\gamma}$ for 0.3% FM-9 is about five times greater than $\dot{\gamma}$ for 0.3% AM-1. (Note that Eq. (14) is here utilized as a constitutive equation assumed approximately valid only in the domain $300 < \dot{\gamma} < 500\,s^{-1}$, $15 < \tau < 25$ dyn/cm^2 for AM-1 and $1100 < \dot{\gamma} < 3500\,s^{-1}$, $10 < \tau < 35$ dyn/cm^2 for FM-9.)

The accuracy of predicting $\dot{\gamma}$ for 0.3% AM-1 can be estimated by considering the data for tensile viscosity η_T given in Ref. 11. It is shown in Ref. 11 that η_T for AM-1 has a strong dependence on the normal deformation rate $\dot{\epsilon}$. Shear viscosity data as a function of shear rate suggest than η_s can be approximated as being independent of $\dot{\gamma}$. Unfortunately, for a non-Newtonian liquid there is no functional relationship between η_T and η_s. However, by assuming Newtonian behavior for any particular domain (recognizing that these domains cannot be directly related), $\eta_T = 3\eta_s$. Then for AM-1, $\eta_T = 0.15$. With this value for η_T (noting an error in Ref. 11 is that concentrations given for AM-1 must be divided by 1.88),[12] $\dot{\epsilon} = 110\,s^{-1}$ is obtained by extrapolation in Fig. 5, Ref. 11 (use 0.16% AM-1). Such an extrapolation is valid on the basis of the experimentally verified, reduced-tensile-viscosity curve for AM-1, using zero shear viscosity as the time-scale reduction parameter, as developed in Ref. 11. By assuming Newtonian behavior near $\eta_T = 0.15$, $\dot{\epsilon} = 110\,s^{-1}$, it follows that $\dot{\gamma} = 110\,s^{-1}$. Further inspection of Fig. 5, Ref. 11 shows that η_T can increase rapidly by orders of magnitude as $\dot{\epsilon}$

is increased less than an order of magnitude. If the tensile viscosity data in Ref. 11 include loading rates representative of those intrinsic to the air-shear test discussed in this paper, $110 < \dot{\gamma} < 1100\ s^{-1}$. From Table 2, $\dot{\gamma} \sim 400\ s^{-1}$. It would appear that the accuracy of $\dot{\gamma}$, using the approximate analytical model, is probably less than a factor of four of the magnitude of the computed value.

Discussion

Several assumptions have been made in order to synthesize an approximate kinematic model of antimisting fuel particles in an airstream under a wing after initial crash impact. The validity of the model to predict d, τ, and $\dot{\gamma}$ was assessed for 0.3% AM-1 fuel on the basis of extrapolation of laboratory data found in Ref. 11. The prediction uncertainty of the model is within an order of magnitude.

The sensitivity of the model to distinguish between AM-1 and FM-9 is demonstrated in Table 2. It remains to be seen if the model is sensitive to changes of test conditions and flow rates planned for in future tests. Although emphasis was placed on examination of the fuel droplet formation shown in Fig. 6, plans exist to collect data to examine that phase from conceptual honeycomb structure to cylinder generation. This phase of the proposed model lends itself well to the work described in Ref. 11.

Examination of Table 1 shows that the leading edge of the antimisting fuel fireball can either accelerate or decelerate and still manifest itself in a fire self-extinction mode. This suggests that there are at least two kinematic mechanisms that can contribute to fire suppression. The role of antimisting agent on these mechanisms will require additional data, such as can be obtained by holography.

The predictions made in Table 2 also suggest that two or more kinematic mechanisms exist. For AM-1, although $\dot{\gamma}$ does not vary significantly, d is different by an order of magnitude. The same observation is made for FM-9. A definite distinction among 0.3% AM-1, 0.3% FM-9, and 0.4% FM-9 is shown by $\dot{\gamma}$ being about 400, 3000, and 2700 s^{-1}, respectively. This is consistent, since the viscosity determines the intrinsic shear strain rate for the particles in the airstream. Furthermore, smaller cylindrical particles have greater surface/volume than larger ones, and are therefore, for a given shear loading, subject to a greater $\dot{\gamma}$. This trend is consistent in Table 2.

The predictions for the different behavior between 0.3% AM-1 and 0.3% FM-9 antimisting fuels are consistent with overall observations. Particles of 0.3% FM-9 are significantly smaller than those of 0.3% AM-1. The model predicts an order of magnitude difference. The shear strain rate for 0.3% AM-1 is predicted to be about an order of magnitude less than that for 0.3% FM-9. This is reasonably confirmed by photographic evidence.

Based on the model, adequate antimisting requires that the average particle diameter be greater than 34 μm, depending on the flow conditions, as compared to that for neat Jet A (~ 0.5 μm). Data from a failure test were used in the model to predict an average particle size in that test of 2 μm. This particular test was not included in this study, since a pool fire under the airfoil obviously influenced the flame front velocity.

It is emphasized that the proposed model is in its embryonic phase of development. Whether or not it can be refined remains to be seen. Its value, at present, is that it does provide some insight into a most complex kinematic problem relatable to fuel expulsion during a survivable aircraft crash landing.

Conclusion

AM-1 and FM-9 antimisting agents in Jet A fuel have been tested in an airstream similar to that for an aircraft survivable crash landing. It was demonstrated that both agents can either self-extinguish or do not propagate fire within the airstream. An approximate model to describe the kinematic behavior of antimisting fuels was synthesized. Experimental results that were exercised with the model suggest that more than one kinematic mechanism can exist that will suppress fire during crash landings.

Acknowledgment

The antimisting fuel testing program was supported by Department of Transportation Contract DOT-FA76WAI-589, T. Horeff and J. Van Dyke program managers. The construction of the diffuser and associated test apparatus was accomplished by M. D. Williams of NWC. Rheological discussions with R. F. Landel of the Jet Propulsion Laboratory, California Institute of Technology, were most valuable.

References

[1] Weatherford, W. D. Jr. and Wright, B. R., "Status of Research on Antimist Aircraft Turbine Engine Fuels in the United States," AGARD/NATO 45th Meeting, Propulsion and Energetics Panel: Aircraft Fire Safety, North Atlantic Treaty Organization, Hartford House, London, April 1975, pp. 2/1-2/8.

[2] Zinn, S., Eklund, T. I., and Neese, W. E., "Photographic Investigation of Modified Fuel Breakup and Ignition," U.S. Dept. of Transportation, Federal Aviation Administration, Washington, D. C., Sept. 1976, Tech. Rept. FAA-RD-76-109, p. 32.

[3] Ahlers, R. H., "Full Scale Aircraft Crash Tests of Modified Jet Fuel," U.S. Dept. of Transportation, Federal Aviation Administration, Washington, D. C., Tech. Rept. FAA-RD-77-13, July 1977, p. 97.

[4] "Crash Survival Design Guide," U.S. Army Air Mobility Research and Development Laboratory, Fort Eustis, Va., Tech. Rept. 71-22, Oct. 1971, p. 373, (AD 733 358).

[5] Personal communication with T. Horeff, Federal Aviation Administration, Washington, D. C.

[6] Dombrowski, N., *Biochemical and Biological Engineering Science*, Vol. 2, Academic Press, New York, 1968, Chap. 16.

[7] Gaydon, A. G. and Wolfhard, H. G., *Flames*, 3rd Ed., Chapman and Hall, London, 1970, p. 81.

[8] Baumeister, T. and Marks, L. S., *Standard Handbook for Mechanical Engineers*, McGraw Hill, New York, 1967, pp. 11-91.

[9] Polymeropoulous, C. E. and Das, S., "The Effect of Droplet Size on the Burning Velocity of Kerosine-Air Sprays," *Combustion and Flame*, Vol. 25, 1975, pp. 247-257.

[10] San Miguel, A., "Inverse Design Criteria for Supersonic Internally Pressurized Polymer Domes," *Journal of Aircraft*, Vol. 13, June 1976, pp. 432-435.

[11] Peng, S. T. J. and Landel, R. F., "Preliminary Investigation of Elongational Flow of Dilute Polymer Solutions," *Journal of Applied Physics*, Vol. 47, Oct. 1976, pp. 4255-4260.

[12] Personal communications with S. T. Peng and R. F. Landel, Jet Propulsion Laboratory, California Institute of Technology, Pasadena, Calif.